MATERIALS
SCIENCE &
ENGINEERING

# Localized deformation via multiple twinning in a Mg–Gd–Y–Zr alloy processed by high-pressure torsion

Lingling Tang [a], Yonghao Zhao [a,*], Ningning Liang [a], R.K. Islamgaliev [b], R.Z. Valiev [b,c], Y.T. Zhu [a,d]

[a] Nano Structural Materials Center, School of Materials Science and Engineering, Nanjing University of Science and Technology, Nanjing 210094, China
[b] Institute of Physics of Advanced Materials, Ufa State Aviation Technical University, 12K. Marx St., Ufa, Russia
[c] Laboratory for Mechanics of Bulk Nanomaterials, Saint Petersburg State University, 28 Universitetsky Prospekt, Peterhof, Saint Petersburg 198504, Russia
[d] Department of Materials Science and Engineering, North Carolina State University, Raleigh, NC 27695, USA

## ARTICLE INFO

## ABSTRACT

Different with common grain refinement dominated by dislocation activities, grain subdivision induced by sequential activation of multiple twinning was observed in a Mg-Gd-Y-Zr magnesium alloy via high-pressure torsion. Deformation bands were evolved from large primary twin bands, which contained refined grains through localized multiple twinning. Nanometer-scaled amorphous bands were also observed within deformation bands in Mg alloys for the first time. These observations indicate that localized deformation via multiple twinning and the consequent formation of deformation bands are potential routes to grain refinement in rare earth-magnesium alloys.

## 1. Introduction

Deformation twinning plays an important role in the plastic deformation of Mg alloys at room temperature, due to their limited number of dislocation slip systems in the hexagonal closed-packed (hcp) crystal structure. Cooperating with dislocation slip to satisfy the von Mises criterion of five independent slip systems, twinning activity can transect large grains, change crystal orientation, and promote dynamic recrystallization [1,2]. The $\{1\,0\,\bar{1}\,2\}\langle1\,0\,\bar{1}\,1\rangle$ extension twins, $\{1\,0\,\bar{1}\,1\}\langle1\,0\,\bar{1}\,2\rangle$ contraction twins and the $\{1\,0\,\bar{1}\,1\}$-$\{1\,0\,\bar{1}\,2\}$ secondary twins are commonly observed after plastic deformation. Nowadays, most of the investigations focused on multiple twinning or activation of various twin variants through electron back scatter diffraction (EBSD) analysis. Martin et al. investigated 36 possible $\{1\,0\,\bar{1}\,1\}$-$\{1\,0\,\bar{1}\,2\}$ twin variants and proposed that the observed secondary twins were almost entirely variants with misorientations of 37.5° or 69.9°, respectively [3]. Mu et al. further pointed out that the Schmidt's law and local strain accommodation were major factors that determined variant selection of primary, secondary and tertiary twins in a deformed Mg alloy [4].

Twinning behaviors varied with different alloying elements, because alloying can change the energy path for twinning and thus affect the twinning tendency [5]. It was reported that deformation twinning was more prevalent in Mg alloys containing rare earth elements (Mg-REs) than it was in other Mg alloys, particularly for the types of contraction twins and the secondary twins [6,7]. Recently, Y element was confirmed to increase the stress required to activate the $\{1\,0\,\bar{1}\,2\}$ twins, and the less common $\{1\,1\,\bar{2}\,1\}$ extension twins were observed in Mg-Y alloys [8]. Moreover, alloying with RE elements was found to increase the number of deformation bands due to the random texture promoted by twinning [9]. Despite that deformation/shear bands always indicate plastic instability or plastic flow localization, deformation bands related to twins in Mg-RE alloys were believed to improve the plasticity for the involved $\langle c+a\rangle$ dislocation slips [10,11]. Stanford et al. pointed out that alloying Mg with Gd and La could produce a new $\{1\,1\,\bar{2}\,1\}$ texture component, which arose from oriented nucleation at shear bands, to weaken the extrusion texture and thus resulted in a good ductility [12].

Among Mg-RE alloy systems, the Mg-Gd-Y-Zr series alloys can provide high strength and high thermal stability at elevated temperatures, due to the aging strengthening, precipitation strengthening, and the relatively stable metastable phases till to 250 °C [13–15]. For example, a Mg-12Gd-3Y-0.6Zr (wt%) alloy by secondary extrusion exhibited a ultimate tensile strength (UTS) of 446 MPa and a yield strength (YS) of 350 MPa along with a elongation of 10.2% at room temperature [15]. Its YS was well above

* Corresponding author.
E-mail address: yhzhao@njust.edu.cn (Y. Zhao).
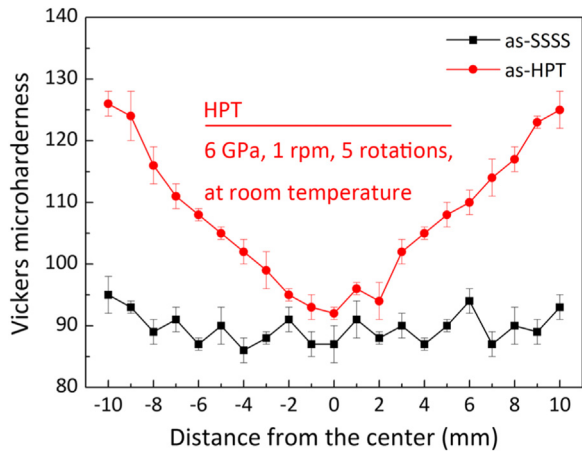
**Fig. 1.** Vickers microhardness of the as-SSSS and as-HPT samples as a function of the distance from the center.

the UTS of most Mg-Al-Zn alloys. Jian et al. reported a Mg-Gd-Y-Ag-Zr alloy with numerous nano-spaced stacking faults, producing a YS as high as 575 MPa [16]. Our previous simulation study indicated that alloying Mg with Gd and Y would decrease the stacking fault energy of basal and prismatic ⟨a⟩ slip, leading to higher probability of non-basal dislocation slip [19]. Additionally, solute atoms Gd and Y were observed to segregate on twinning boundaries, which influenced the twinning activities in turn [8,17,18]. Deformation bands and deformation twins were also observed in a Mg-9Gd-4Y-0.6Zr alloy under uniaxial hot compression [20]. It seems that the appearance of deformation band was generally associated with deformation twins in Mg-RE alloys. While, up to date, the intrinsic relationship between deformation band and deformation twins is undefined. Moreover, these deformation bands and twinning behaviors were mainly observed under traditional deformations, such as hot extrusion, compression and rolling. The alloying effects of Gd and Y on the deformation twinning under server plastic deformation (SPD) are still unclear, such as high-pressure torsion (HPT), equal channel angular pressing etc.

It is known that HPT exerts high hydrostatic pressure, which makes it possible to impose high shear strain and produce finer grains than other SPD techniques. In this study, a Mg-Gd-Y-Zr alloy was subjected to HPT processing at room temperature. Different

from traditional deformation dominated by dislocation slips under HPT processing, a large number of localized multiple twins were introduced and investigated. Furthermore, the special grain refinement pattern by multiple twinning and the alloying effects of Gd and Y on the deformation twinning were discussed.

## 2. Experimental

An ingot with a nominal composition of Mg-8Gd-3Y-0.4Zr (wt%) was extruded at 480 °C with extrusion ratio of 9:1. Before subjected to HPT processing, sample disks with a diameter of 20 mm and thickness of 1 mm were sectioned vertical to extrusion direction and then homogenization treatment was carried out at 500 °C for 12 h to obtain supersaturated solid solution (denoted as-SSSS). The HPT processing was conducted at room temperature under quasi-constrained conditions using a pressure of 6.0 GPa and a rotational speed of 1 rpm up to 5 rotations (denoted as-HPT).

After HPT processing, the disks were mechanically polished to a mirror-like finish and then etched with acetic picral (5 g of picric acid, 10 mL of acetic acid, 10 mL of water and 100 mL of ethanol) for optical microscopy (OM) observation through a true color confocal microscope system (Axio CSM 700). A Zeiss Auriga field emission scanning electron microscope (SEM) equipped with an Oxford HKL Channel 5 system was employed for SEM and EBSD analysis. The EBSD samples of as-SSSS and as-HPT were both sectioned at the radius of 5 mm and prepared by electro polishing using a standard Struers AC2 electrolyte at a voltage of 20 kV and a temperature of −30 °C. The applied EBSD scanning step size was 0.1 μm with a voltage of 20 kV. The calibration rate of the as-SSSS and as-HPT samples reached 97% and 82% respectively, thus the showing EBSD images were original without any optimization. Considering the limitations of spatial revolution and stress effect of the EBSD technique, we further identified the microstructure of samples at radius of 5 mm by an aberration corrected transmission electron microscopy (TEM) (Titan G2 60-300) at 300 kV. The TEM samples were pre-thinned by twin-jet polishing at 18 kV and −30 °C using a solution containing 5% perchloric acid and 95% ethanol, and followed by precision ion milling (GATAN 691) until final penetration. The distribution of the Vickers microhardness across the diameter of a disk was measured for four times with a HMV-G 21DT (Shimazdu, Japan) equipment at the load of 980 mN and dwelling time of 10 s.
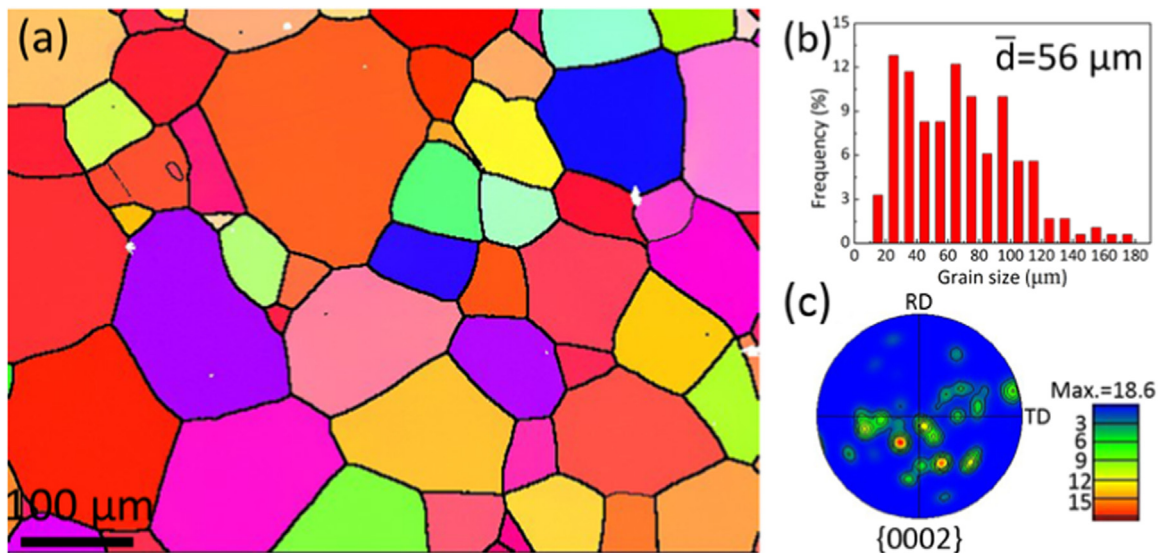


**Fig. 2.** EBSD analysis of the as-SSSS sample. (a) Inverse polar figure (IPF). (b) Plot of the frequencies of occurrence (%) vs. grain size (μm). (c) The {0002} polar figure.
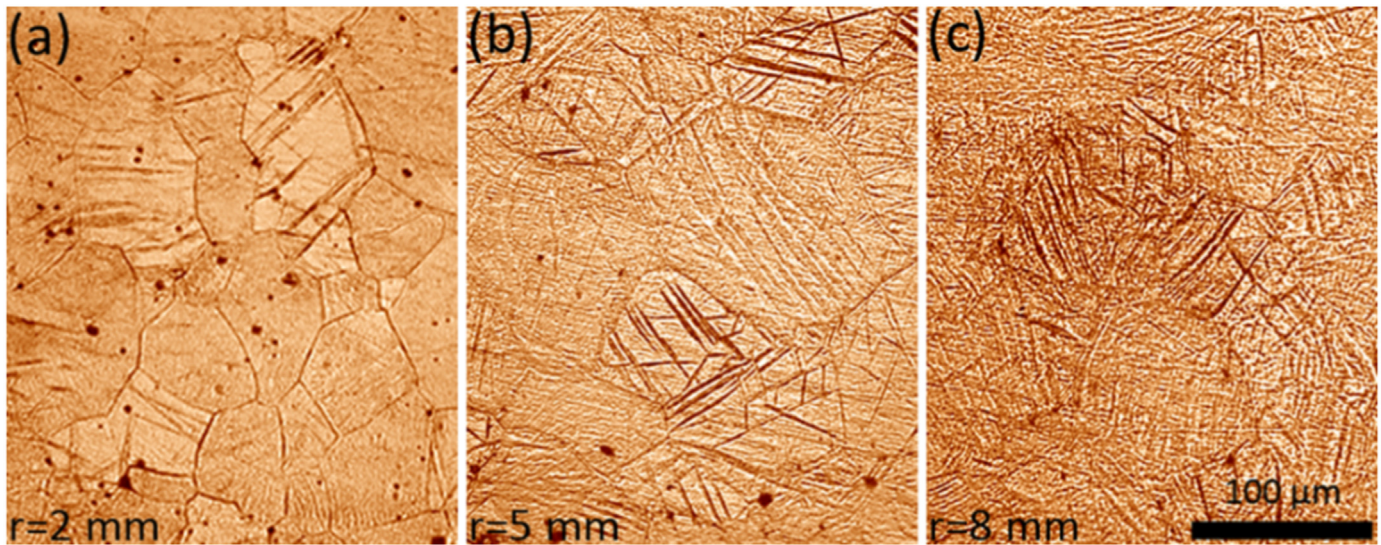
**Fig. 3.** Optical microscopy images of the microstructure evolution at radius of 2, 5 and 8 mm for the as-HPT sample.
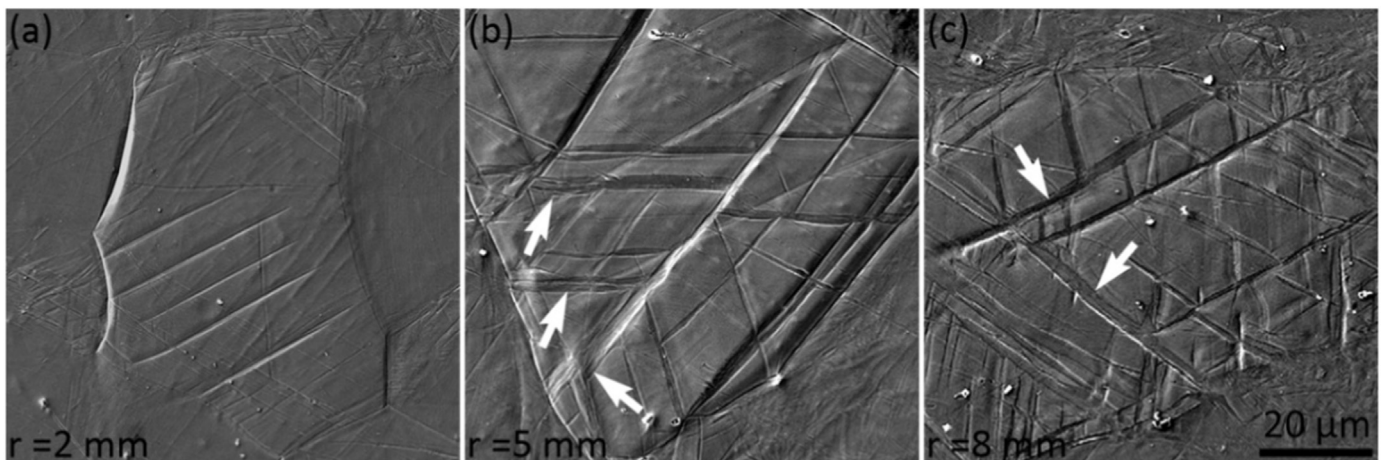


**Fig. 4.** SEM images of the microstructure evolution at radius of 2, 5 and 8 mm for the as-HPT sample; twins with uneven morphologies are indicated by white arrows.

## 3. Results and discussion

Fig. 1 shows the Vickers microhardness distribution of the as-SSSS and as-HPT samples along the diameter. The as-SSSS sample exhibited quite a uniform microhardness value ($\sim$90 Hv). Compared with the as-SSSS sample, the microhardness of the as-HPT sample gradually increased from 90 to 125 Hv with the radius (r) from the center (0 mm) to the periphery (10 mm). It is worth noting that the high microhardness value of 125 Hv is comparable with that of the ultrafine grained or even nanocrystalline [21,22]. The estimated equivalent strain ($\varepsilon$) on the periphery of the disk at r = 10 mm was $\sim$6.3 according to the equitation $\varepsilon = \ln\left(2\pi Nrh_0/h^2\right)$ [23], where N is the number of torsional revolutions, r is the radius of the disk (N = 5, r = 10 mm), $h_0$ and h are the thickness of the disk before and after HPT processing ($h_0$ = 1 mm, h = 0.75 mm).

To elucidate the unusual microhardness distribution after HPT processing, we performed microstructure observations along the radius. EBSD inverse polar figure (IPF) of the as-SSSS sample is displayed in Fig. 2(a). Most grains were equiaxed in range of 20–120 $\mu$m and the average grain size was measured to be 56 $\mu$m (Fig. 2b). It is known that Mg alloys subjected to extrusion are prone to form the basal texture, which has significant influence on the subsequent deformation behaviors and mechanical properties

[24]. In the {0 0 0 2} polar figure (Fig. 2c), two weak pyramidal orientation regions were observed, and no obvious texture could be found. In fact, previous studies proved that Mg alloying with REs can efficiently weaken extrusion texture, to form a weak RE component texture [12,25], which could be eliminated by the subsequent homogenization treatment. Thus, the texture influence on deformation behaviors of the as-HPT sample was negligible in present study.

Fig. 3 shows the OM observations of the as-HPT sample at r = 2, 5 and 8 mm. Results suggested that twinning formed in a few large grains at r = 2 mm, which were initiated from grain boundaries and parallel with each other; with increasing local strain at r = 5 mm, twinning that initiated from other directions in the same grain was activated; when r reached 8 mm, grains were further divided into smaller domains and the initial large grains can barely be observed. These OM observations were further verified by SEM observations at r = 2, 5 and 8 mm. As shown in SEM images (Fig. 4), some wide twins featured uneven morphologies (marked by white arrows), which was similar with the twinning morphology observed in a rolled AZ31 alloy [26]. This will be discussed later. Clearly, twinning deformation occurred overwhelmingly at room temperature, although the critical resolved shear stress for activating twinning was reported to be several times higher than that for dislocation slips [27]. The imposed strain by HPT increased
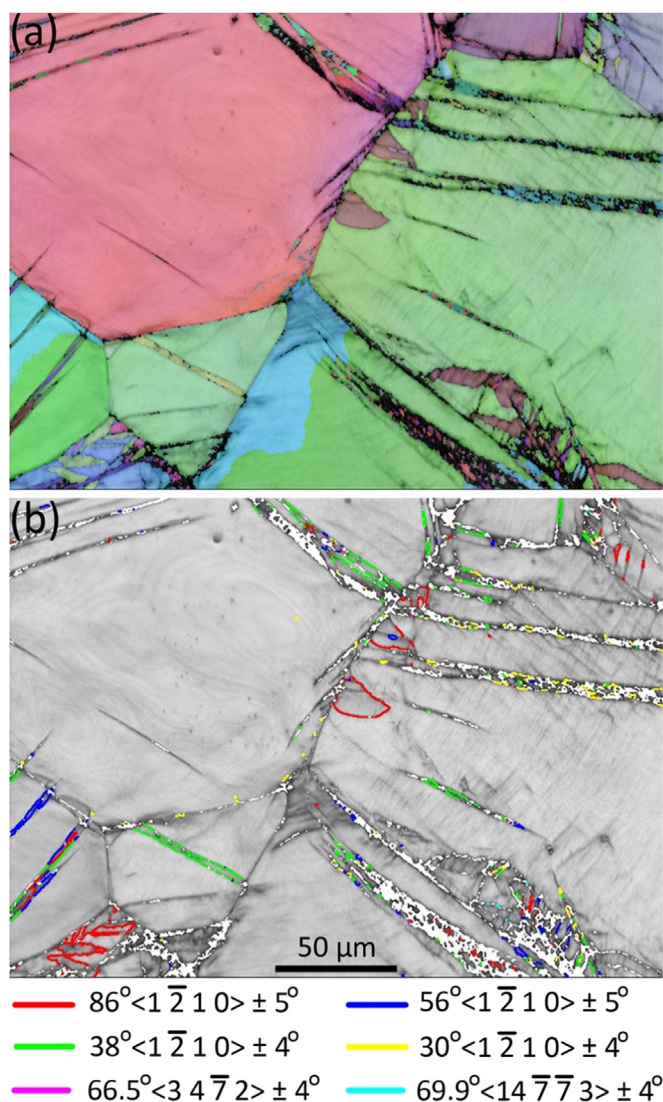
**Fig. 5.** EBSD (a) inverse polar figure (IPF) and (b) Kikuchi band contrast map of the as-HPT sample at the radius of 5 mm. The {1 $\bar{2}$ 1 0} extension twin and {1 0 $\bar{1}$ 1} contraction twin boundaries are shown in red (86°⟨1 $\bar{2}$ 1 0⟩ ± 5°) and blue (56°⟨1 $\bar{2}$ 1 0⟩ ± 5°); the colors of secondary twin boundaries associated with four variants are denoted in the legend. (For interpretation of the references to color in this figure legend, the reader is referred to the web version of this article).

with the disk radius and thereby the amount of activated twins grew along the radius direction. As a result, grain refining was determined by the capacity of deformation twins in dividing grains. Thus, the variable distribution of microhardness values was attributed to the gradient grain subdivision along the radius.

To further study the grain subdivision by multiple twinning, the as-HPT sample was investigated using EBSD method, as shown in Fig. 5. Large numbers of the primary twins were nucleated from grain boundaries in parallel, forming long and narrow twin bands (Fig. 5a). During twinning, localized stresses were generated at twin tips and such stress localization catalyzed nucleation of new twins [28]. Extensive secondary twins were subsequently activated to divide grains in these twin bands, which may explain the observed uneven morphology in SEM images (Fig. 4). Fig. 5b shows the corresponding EBSD Kikuchi band contrast map to highlight these different twins. Extension twin and contraction twin boundaries as well as secondary twin boundaries that associated with four variants were detected and marked with different colors. Most secondary twins were variants of 38°⟨1 $\bar{2}$ 1 0⟩ ± 4° (in green) and 30°⟨1 $\bar{2}$ 1 0⟩ ± 4° (in yellow), abiding by the high

Schmidt factor rule [3]. Though with low Schmidt factors, a few variants 66.5°⟨3 4 $\bar{7}$ 2⟩ ± 4° (in fuchsia) and 69.9°⟨14 $\bar{7}$ $\bar{7}$ 3⟩ ± 4° (in aqua) were detected at interaction regions of several twin bands or at triple junctions of grain boundaries, which indicated the localized strain accommodation. During deformation, shear strains was released through multiple twinning. However, dislocation activities would be inevitably activated, which took main responsibility for the low Kikuchi pattern calibration rate in twinning deformation regions.

Fig. 6a shows a TEM bright field image of typical microstructures within a large primary twin. Small grains (G3 and G4) can be seen in the primary twin grain (G2). Viewed from the ⟨1 $\bar{2}$ 1 0⟩ zone axis, high-resolution TEM (HREM) and the corresponding diffraction pattern revealed the twin orientation relationship of 86°⟨1 $\bar{2}$ 1 0⟩ between the G2 and G3, and 56°⟨1 $\bar{2}$ 1 0⟩ between the G1 and G3 (Fig. 6b). However, the grain boundary angle between G2 and G4 was measured to be 13.9°. Clearly, the formation of G3 was caused by twinning, while the existence of G4 could only be explained by grain reorienting to accommodate the surrounding twinning deformation. Formation of similar grains was observed in a rolled Mg alloy, which was induced by grain reorientation of two and three twinning events [18]. Evidently, we have confirmed that small grain segments within the large primary twins were induced by multiple twinning with the help of grain reorientation.

Apart from the isolated large twins, plenty of narrow twins were propagated from different orientations and strongly interacted with each other. Fig. 7a shows several narrow twins that were nucleated from the grain boundary in parallel; at the other side of the grain boundary, a deformation band (more than 2 μm wide) was formed (Fig. 7b). The diffraction pattern of the white circle region confirmed the polycrystalline structure in the deformation band. Fig. 7c shows the intersected twins inside a big grain: new small grains appeared at the cross region of two twins (in black dotted circle). The twin in the center was slightly bent due to deformation; a black block in different contrast with the parent twin may suggest the change in crystal orientation. The detailed microstructure of the dashed twin band was shown in Fig. 7d, which is similar with the deformation band in Fig. 7b. A continuous band consisting of the {1 0 $\bar{1}$ 2}⟨1 0 $\bar{1}$ $\bar{1}$⟩ twin variants, which are connected with the grain boundaries, was reported in a AZ31 Mg sheet bending [29]. However, deformation bands, which evolved from localized multiple twinning, have not been reported yet. Moreover, this type of deformation bands is more like a stream banding with obvious plastic flow traces, which can be frequently observed in the early plastic deformation dominated by dislocation activities [30]. A transition from twinning to basal slip, localized along deformation bands, has been found to take place with decreasing grain size in pure Mg [26]. Zhao et al. reported that a single-crystal aluminum, which usually deform by dislocation slip, started to twin and even formed shear bands to accommodate the flow [31]. Whether the dislocation slip was activated later within the deformation bands to form such stream bandings needs to be further investigated. Combining with EBSD results and TEM observations above, it appears that deformation bands were generated by grain subdivisions via secondary twinning within the large primary twin bands.

Fig. 8a shows a narrow white band with a width over 20 nm within a deformation band. A similar band can be also found in Fig. 7d, as marked by a white arrow. Fig. 8b displays the HREM image of the white rectangle area, revealing the existence of an amorphous phase. In its corresponding diffraction pattern, the halo appearance further confirmed the amorphous nature of the band. Localized amorphization induced by severe plastic deformation have been reported in Cu alloys [32] and Al alloys [33], yet it has not been reported in Mg alloys. Amorphization process is commonly regarded as a solid-state transformation [34]. Huang
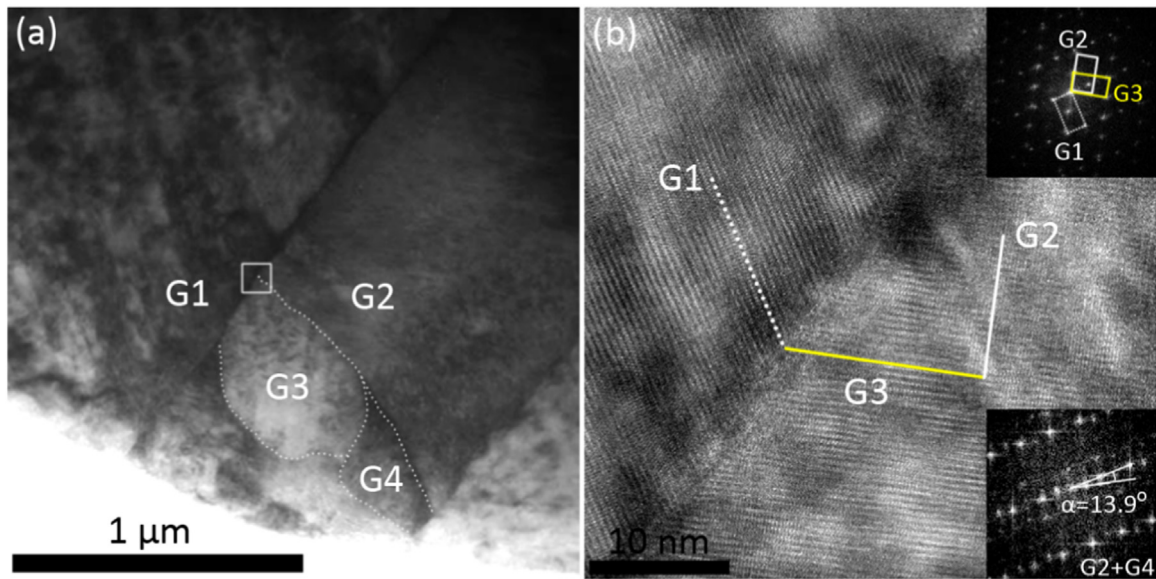
**Fig. 6.** (a) TEM bright field image of microstructure within the primary twin band. (b) HREM image of white square region in (a) with its corresponding diffraction pattern (inset in the upper right) of G1, G2 and G3; diffraction pattern of G2 and G4 (inset in the lower right).
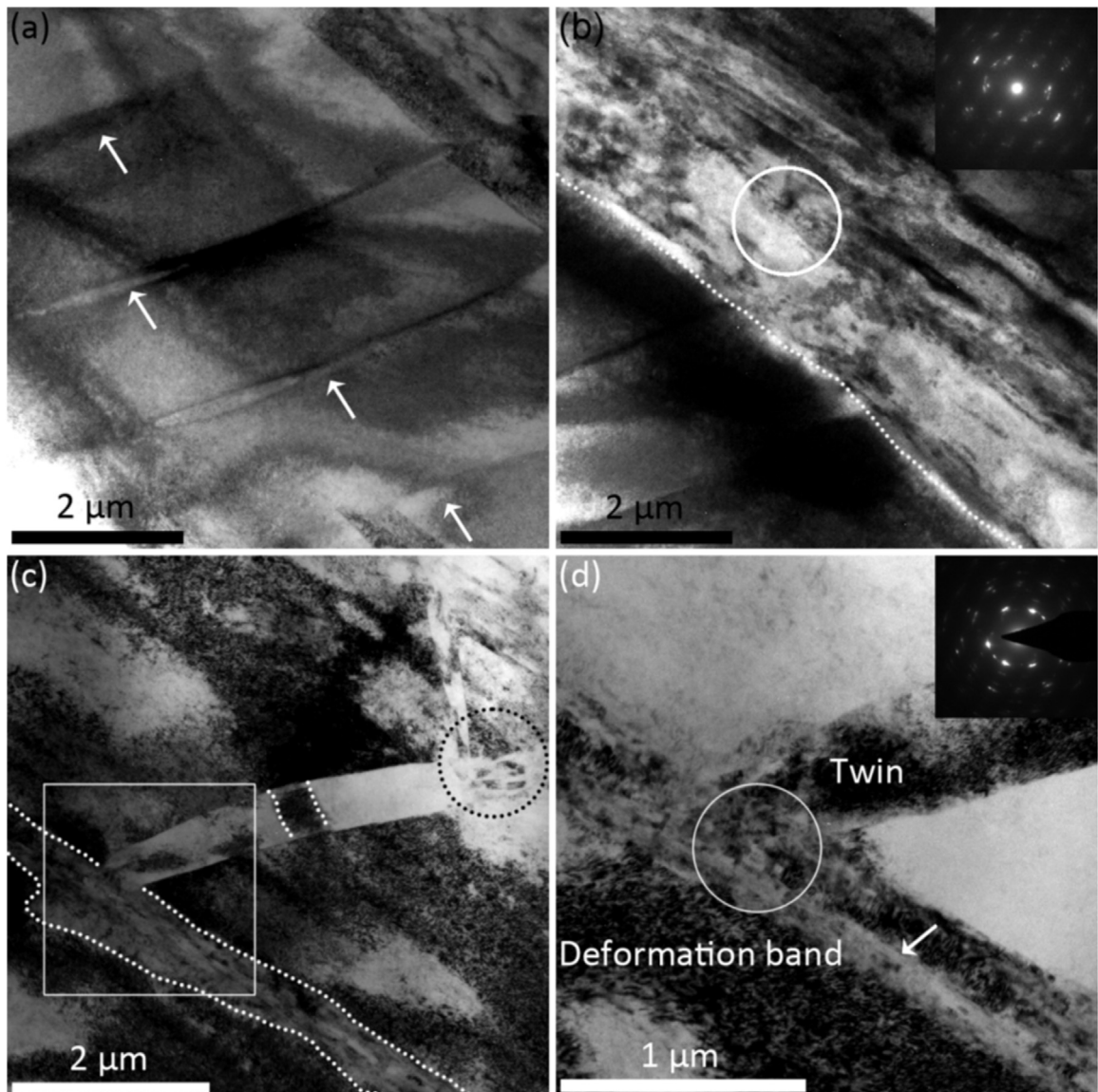


**Fig. 7.** Observed (a) parallel twins and (b) deformation band at both sides of a grain boundary. (c) Interaction region of multiple twinning. (d) Deformation band induced by multiple twinning at white square region in (c).
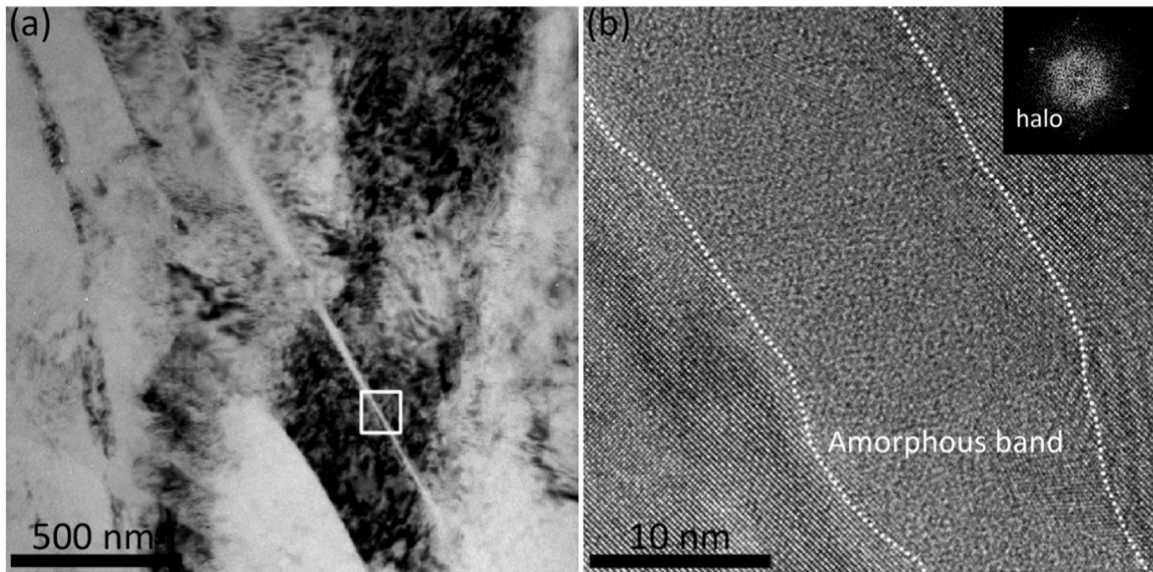
**Fig. 8.** (a) Amorphous band within the deformation band. (b) HREM image at white square region in (a) with the corresponding diffraction pattern.
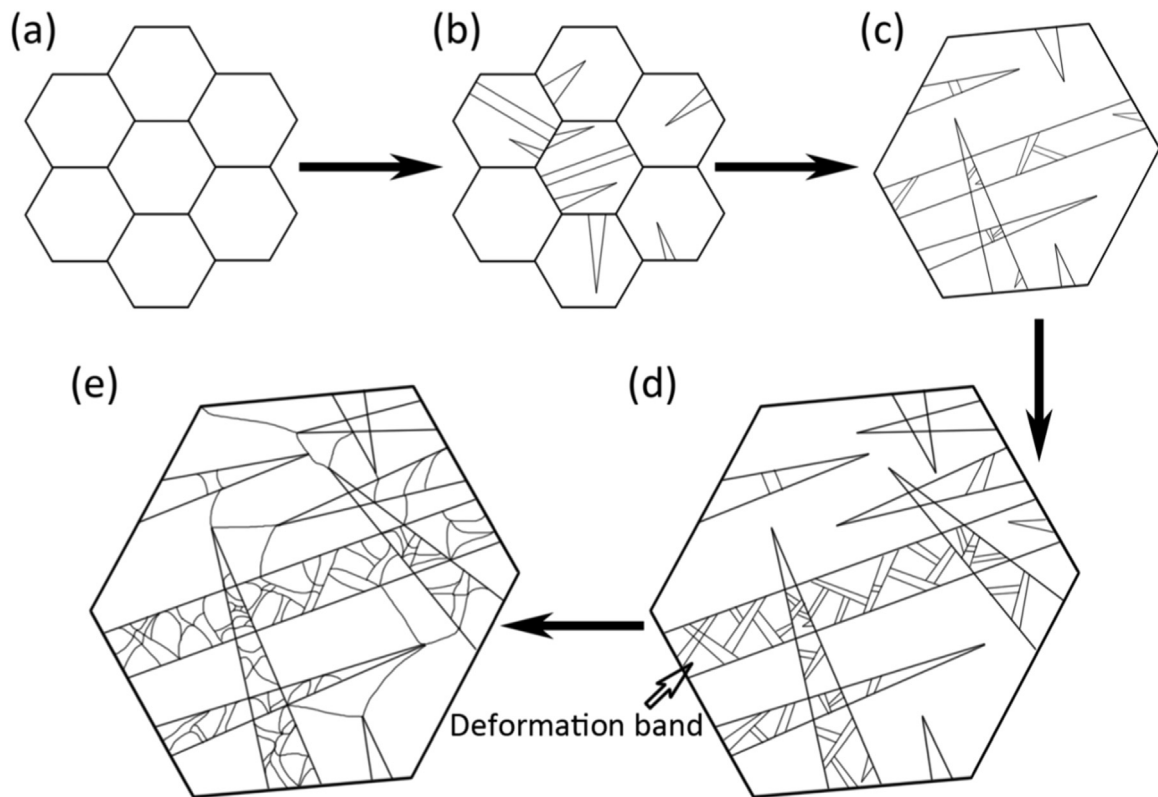


**Fig. 9.** Schematic of the grain subdivision via the sequential activation of localized multiple twinning and forming deformation band.

et al. investigated a TiNi alloy processed by HPT, and pointed out that the deformation-induced amorphization initiated from dislocation core regions in the interior of grains and from grain boundaries [35]. The accumulated dislocations at multiple twinning boundaries in deformation band may be the reason for the formation of amorphous phase.

A schematic diagram of the grain subdivision via the sequential activation of localized multiple twinning and forming deformation band was depicted in Fig. 9. In early stage of deformation, primary twins were initiated from grain boundaries and parallel with each other (Fig. 9b). With increasing strain, twinning formed in different directions in a same grain (Fig. 9c). In some large twins, large numbers of secondary twins were activated to further cut these grains, thus forming localized deformation bands, as shown in Fig. 9d. Through localized deformation of multiple twinning, localized grain refinement can be firstly obtained in the deformation bands. Twinning deformation is essentially associated with strain accommodation along c-axis direction, thus imposed stress can be gradually relaxed by localized multiple twinning or even by activation of non-basal slips, which enables the subsequent plastic deformation. In this way, a large grain can be divided into small grains (Fig. 9e). With further straining, as

supported by the high Hv values (120–125 Hv) at radius of 9 and 10 mm, uniform refinement of all large grains is promising. Thus, grain subdivision can be completed on a step-wise approach of regional grain refinements through localized multiple twinning and forming deformation bands.

Recently, superplasticity of a nano-grained Mg–9Gd–4Y–0.4Zr alloy subjected to high-pressure torsion was obtained and extensive deformation twins were observed prior to the homogeneous nanocrystalline microstructure [36]. It's noticeable that extent of grain refinement in Mg-Al-Zn alloys by HPT was confined to ultrafine level and the refining process was mainly controlled by dislocation activities. Lentz et al. proposed a potential strengthening mechanism resulted from the similar microstructure with {1 0 $\bar{1}$ 1}-{1 0 $\bar{1}$ 2} double twins networks [37]. Besides, deformation band in Mg-RE alloys could also improve the plasticity by weakening texture [12]. In other words, these deformation twins in Mg-RE alloys benefited the improvement of plastic property. According to previous research, deformation band in Mg-RE alloys mainly consisted of dynamic recrystallization grains [2,9,12]. While, all these tests were conducted under elevated temperature that favored the dynamic recrystallization. In this work, the HPT deformation was carried at room temperature, thus the localized multiple twinning remained. Similar phenomenon that deformation twins were substituted with extensive recrystallized deformation bands with the increasing temperatures was reported in a Mg-9Gd-4Y-0.6Zr alloy [20]. Consequently, it is suspected that these deformation bands naturally initiated from the localized multiple twinning.

On basis of the above discussion, it can be concluded that the localized multiple twinning played a crucial role in the microstructure evolution. As known, alloying can promote twin nucleation and twin growth through lowering stacking fault energy and twin fault energy at the twin boundary. More than 30% reduction of stacking fault energy for growth fault and deformation fault was reported by Mg alloying with Y [38]. In a Mg-Gd-Y-Ag-Zr alloy, Zhou et al. pointed out that interfacial energies could be changed by segregation with Gd in sequence of grain boundary > twin boundary > stacking fault [18]. Furthermore, Gd and Y solute atoms may influence the atomic shuffling process during twinning shear and thereby change the stress required to activate deformation twins [8]. Thus, the massive twinning in priority of dislocation slips can be mainly attributed to the alloying of Gd and Y elements. In addition, HPT processing can effectively suppress the crack propagation, which helps with building up high local stresses to activate multiple twinning without cracking [39].

## 4. Conclusions

In this work, the deformation behaviors of a Mg-8Gd-3Y-0.4Zr alloy processed by HPT at room temperature were investigated. Microstructure observations revealed that the successive grain subdivision through increasing deformation twinning led to the variable Hv microhardness values. Deformation bands were confirmed to evolve from localized multiple twinning and mainly consisted of four {1 0 $\bar{1}$ 1}-{1 0 $\bar{1}$ 2} double twin variants. These observations indicate that localized deformation of multiple twinning and forming deformation bands are potential routes to grain refinement of Mg-RE alloys. Furthermore, alloying of Gd and Y played a significant role in the formation of deformation twins and deformation bands.

## Acknowledgement

## References

[1] X.Z. Liao, J. Wang, J.F. Nie, Y.Y. Jiang, P.D. Wu, Deformation twinning in hexagonal materials, MRS Bull. 41 (2016) 314–319.

[2] R. Cottam, J. Robson, G. Lorimer, B. Davis, Dynamic recrystallization of Mg and Mg–Y alloys: crystallographic texture development, Mater. Sci. Eng. A 485 (2008) 375–382.

[3] É. Martin, L. Capolungo, L. Jiang, J.J. Jonas, Variant selection during secondary twinning in Mg-3% Al, Acta Mater. 58 (2010) 3970–3983.

[4] S. Mu, J.J. Jonas, G. Gottstein, Variant selection of primary, secondary and tertiary twins in a deformed Mg alloy, Acta Mater. 60 (2012) 2043–2053.

[5] S.L. Shang, W.Y. Wang, B.C. Zhou, Y. Wang, K.A. Darling, L.J. Kecskes, S. N. Mathaudhu, Z.K. Liu, Generalized stacking fault energy, ideal strength and twinnability of dilute Mg-based alloys: a first-principles study of shear deformation, Acta Mater. 67 (2014) 168–180.

[6] M.R. Barnett, M.D. Nave, C.J. Bettles, Deformation microstructures and textures of some cold rolled Mg alloys, Mater. Sci. Eng. A 386 (2004) 205–211.

[7] X. Hou, Z. Cao, X. Sun, L. Wang, L. Wang, Twinning and dynamic precipitation upon hot compression of a Mg-Gd-Y-Nd-Zr alloy, J. Alloy. Compd. 525 (2012) 103–109.

[8] N. Stanford, R.K.W. Marceau, M.R. Barnett, The effect of high yttrium solute concentration on the twinning behaviour of magnesium alloys, Acta Mater. 82 (2015) 447–456.

[9] K. Hantzsche, J. Bohlen, J. Wendt, K. Kainer, S. Yi, D. Letzig, Effect of rare earth additions on microstructure and texture development of magnesium alloy sheets, Scr. Mater. 63 (2010) 725–730.

[10] J.P. Hadorn, K. Hantzsche, S. Yi, J. Bohlen, D. Letzig, J.A. Wollmershauser, S. R. Agnew, Role of solute in the texture modification during hot deformation of Mg-rare earth alloys, Metall. Mater. Trans. A 43 (2011) 1347–1362.

[11] S. Sandlöbes, S. Zaefferer, I. Schestakow, S. Yi, R. Gonzalez-Martinez, On the role of non-basal deformation mechanisms for the ductility of Mg and Mg-Y alloys, Acta Mater. 59 (2011) 429–439.

[12] N. Stanford, M. Barnett, The origin of "rare earth" texture development in extruded Mg-based alloys and its effect on tensile ductility, Mater. Sci. Eng. A 496 (2008) 399–408.

[13] S.M. He, X.Q. Zeng, L.M. Peng, X. Gao, J.F. Nie, W.J. Ding, Precipitation in a Mg-10Gd-3Y-0.4Zr (wt%) alloy during isothermal ageing at 250 °C, J. Alloy. Compd. 421 (2006) 309–313.

[14] S.M. He, X.Q. Zeng, L.M. Peng, X. Gao, J.F. Nie, W.J. Ding, Microstructure and strengthening mechanism of high strength Mg-10Gd-2Y-0.5Zr alloy, J. Alloy. Compd. 427 (2007) 316–323.

[15] X. Li, W. Qi, K. Zheng, N. Zhou, Enhanced strength and ductility of Mg-Gd-Y-Zr alloys by secondary extrusion, J. Magnes. Alloys 1 (2013) 54–63.

[16] W.W. Jian, G.M. Cheng, W.Z. Xu, H. Yuan, M.H. Tsai, Q.D. Wang, C.C. Koch, Y. T. Zhu, S.N. Mathaudhu, Ultrastrong Mg alloy via nano-spaced stacking faults, Mater. Res. Lett. 1 (2013) 61–66.

[17] J.F. Nie, Y.M. Zhu, J.Z. Liu, X.Y. Fang, Periodic segregation of solute atoms in fully coherent twin boundaries, Science 340 (2013) 957–960.

[18] H. Zhou, G.M. Cheng, X.L. Ma, W.Z. Xu, S.N. Mathaudhu, Q.D. Wang, Y.T. Zhu, Effect of Ag on interfacial segregation in Mg-Gd-Y-(Ag)-Zr alloy, Acta Mater. 95 (2015) 20–29.

[19] L.L. Tang, W. Liu, Z.G. Ding, D.L. Zhang, Y.H. Zhao, E.J. Lavernia, Y.T. Zhu, Alloying Mg with Gd and Y: Increasing both plasticity and strength, Comp. Mater. Sci. 115 (2016) 85–91.

[20] L. Li, Deformation band and texture of a cast Mg-RE alloy under uniaxial hot compression, Mater. Sci. Eng. A 528 (2011) 7178–7185.

[21] Y. Kawamura, K. Hayashi, A. Inoue, T. Masumoto, Rapidly solidified powder metallurgy $Mg_{97}Zn_1Y_2$ alloys with excellent tensile yield strength above 600 MPa, Mater. Trans. 42 (2001) 1171–1174.

[22] J. Čížek, I. Prochazka, B. Smola, I. Stulíková, R. Kužel, Z. Matěj, V. Cherkaska, R. K. Islamgaliev, O. Kulyasova, Microstructure and thermal stability of ultra fine grained Mg-based alloys prepared by high-pressure torsion, Mater. Sci. Eng. A 462 (2007) 121–126.

[23] A.P. Zhilyaev, T.G. Langdon, Using high-pressure torsion for metal processing: Fundamentals and applications, Prog. Mater. Sci. 53 (2008) 893–979.

[24] T. Homma, N. Kunito, S. Kamado, Fabrication of extraordinary high-strength magnesium alloy by hot extrusion, Scr. Mater. 61 (2009) 644–647.

[25] N. Stanford, D. Atwell, A. Beer, C. Davies, M.R. Barnett, Effect of microalloying with rare-earth elements on the texture of extruded magnesium-based alloys, Scr. Mater. 59 (2008) 772–775.

[26] C.M. Cepeda-Jiménez, J.M. Molina-Aldareguia, M.T. Pérez-Prado, Origin of the twinning to slip transition with grain size refinement, with decreasing strain rate and with increasing temperature in magnesium, Acta Mater. 88 (2015) 232–244.

[27] X. Lou, M. Li, R. Boger, S. Agnew, R. Wagoner, Hardening evolution of AZ31B Mg sheet, Int. J. Plast. 23 (2007) 44–86.

[28] M.A. Kumar, A. Kanjarla, S. Niezgoda, R. Lebensohn, C. Tomé, Numerical study of the stress state of a deformation twin in magnesium, Acta Mater. 84 (2015) 349–358.

[29] J. Baird, B. Li, S.Y. Parast, S. Horstemeyer, L. Hector, P. Wang, M. Horstemeyer, Localized twin bands in sheet bending of a magnesium alloy, Scr. Mater. 67 (2012) 471–474.

[30] Q. Xue, G. Gray III, Development of adiabatic shear bands in annealed 316L stainless steel: Part II. TEM studies of the evolution of microstructure during deformation localization, Metall. Mater. Trans. A 37 (2006) 2447–2458.

[31] F. Zhao, L. Wang, D. Fan, B. Bie, X. Zhou, T. Suo, Y. Li, M. Chen, C. Liu, M. Qi, Macro deformation twins in single-crystal aluminum, Phys. Rev. Lett. 116 (2016) 075501.

[32] S. Ohsaki, S. Kato, N. Tsuji, T. Ohkubo, K. Hono, Bulk mechanical alloying of Cu–Ag and Cu/Zr two-phase microstructures by accumulative roll-bonding

process, Acta Mater. 55 (2007) 2885–2895.

[33] X. Wu, N. Tao, Y. Hong, J. Lu, K. Lu, Localized solid-state amorphization at grain boundaries in a nanocrystalline Al solid solution subjected to surface mechanical attrition, J. Phys. D: Appl. Phys. 38 (2005) 4140.

[34] M. Chen, J.W. McCauley, K.J. Hemker, Shock-induced localized amorphization in boron carbide, Science 299 (2003) 1563–1566.

[35] J.Y. Huang, Y.T. Zhu, X.Z. Liao, R.Z. Valiev, Amorphization of TiNi induced by high-pressure torsion, Philos. Mag. Lett. 84 (2004) 183–190.

[36] R. Alizadeh, R. Mahmudi, A.H.W. Ngan, Y. Huang, T.G. Langdon, Superplasticity of a nano-grained Mg-Gd-Y-Zr alloy processed by high-pressure torsion, Mater. Sci. Eng. A 651 (2016) 786–794.

[37] M. Lentz, M. Risse, N. Schaefer, W. Reimers, I. Beyerlein, Strength and ductility with $\{10\bar{1}1\}$-$\{10\bar{1}2\}$ double twinning in a magnesium alloy, Nat. Commun. 7 (2016).

[38] W.Y. Wang, S.L. Shang, Y. Wang, Z.G. Mei, K.A. Darling, L.J. Kecskes, S. N. Mathaudhu, X.D. Hui, Z.K. Liu, Effects of alloying elements on stacking fault energies and electronic structures of binary Mg alloys: a first-principles study, Mater. Res. Lett. 2 (2014) 29–36.

[39] Y. Huang, R.B. Figueiredo, T. Baudin, F. Brisset, T.G. Langdon, Evolution of strength and homogeneity in a magnesium AZ31 alloy processed by high-pressure torsion at different temperatures, Adv. Eng. Mater. 14 (2012) 1018–1026.